



# Quantitative analysis of titanium alloys using one-point calibration laser-induced breakdown spectroscopy

Ran Hai<sup>1</sup> · Weina Tong<sup>1</sup> · Ding Wu<sup>1</sup> · Zhonglin He<sup>1</sup> · Harse Sattar<sup>1</sup> · Cong Li<sup>1</sup> · Hongbin Ding<sup>1</sup>

Received: 22 August 2020 / Accepted: 23 January 2021 / Published online: 20 February 2021  
© The Author(s), under exclusive licence to Springer-Verlag GmbH, DE part of Springer Nature 2021

## Abstract

The development of real-time and on-line quantitative composition analysis is desired for the products quality improvement in the metal producing and processing industries. Accuracy is still a challenge for classical calibration-free laser-induced breakdown spectroscopic (CF-LIBS) quantitative analysis due to the influence of the inaccurate plasma temperature calculations, uncertainties associated with Einstein coefficients and imprecise efficiency of spectral detection system. In this paper, we present an improving quantitative analysis for both major and minor elements in titanium alloys using the one-point calibration LIBS (OPC-LIBS) method. In OPC-LIBS, one matrix-matched standard sample of known composition was used to synchronously correct the essential experimental and spectroscopic parameters. A Saha–Boltzmann plot covering a large energy range was used to obtain more accurate plasma temperature and electron density values. From the comparison results, the OPC-LIBS method leads to a more accurate determination of the titanium alloy composition compared with the conventional CF-LIBS approach.

## 1 Introduction

Titanium alloys are excellent candidates for aerospace applications owing to their excellent corrosion resistance and high strength to weight ratio [1]. Additionally, titanium alloys are of uttermost interest with regard to additive manufacturing (AM), which has lately become an option for metal parts production directly from three-dimensional digital models as well as express and economy remanufacturing of broken parts [2]. The development of real-time, online sensing, and closed-loop control system is essential for the products quality improvement as well as advancement of AM into high-value applications where component failure due to element segregation cannot be tolerated. The continuously increasing requirements for product quality in AM industries initiate the demand for measuring methods having the potential to analyze the chemical composition of the processed materials at high speed and—if possible—on-line. However, there are few investigations focused on in-situ composition

monitoring of the AM processes [3, 4]. Laser-induced breakdown spectroscopy (LIBS) is predestined for this task, in which study of characteristic line emission from the laser-induced plasma can give information about the composition of the sample material [5, 6]. As in most analytical methods, quantitative LIBS analysis usually relies upon the use of calibration curves about the intensity to concentration or mass relationship. But in some conditions, it can be problematic obtaining enough matrix-matched standards for establishing a suitable calibration curve. In comparison, the calibration-free LIBS (CF-LIBS) approach, developed by Ciucci et al. [7] in 1999, is based on the measurement of line intensities and plasma parameters (plasma electron density and temperature) and on the assumption of a Boltzmann population of excited levels to calculate multi-elemental concentrations, which overcomes the limitation of using matrix-matched standards and avoids the need for any comparison with calibration curves. Due to its unique features, CF-LIBS has been widely applied for the quantitative analysis in material science [8–11], biomedicine [12–14], environmental monitoring [15–17], space exploration [18, 19], and so on. LIBS has shown a strong potential for quantitative analysis for on-line, stand-off and in real time. The precision and accuracy of CF-LIBS results can be compromised by uncertainties associated with matrix effects, Einstein coefficients  $A_{ki}$  (up to 50% [20]) and efficiency of spectral detection system

✉ Hongbin Ding  
hding@dlut.edu.cn

<sup>1</sup> Key Laboratory of Materials Modification By Laser, Ion and Electron Beams, Chinese Ministry of Education, School of Physics, Dalian University of Technology, Dalian 116024, People's Republic of China

$F(\lambda)$ . To improve the analytical performances of CF-LIBS, Cavalcanti et al. [21] developed the one-point calibration LIBS (OPC-LIBS) in 2013. The main idea behind OPC-LIBS method is using only one matrix-matched standard sample of known composition to calculate comprehensive correction factors  $P(\lambda)$  for empirically correcting the LIBS line intensities in Boltzmann plots. The selected standard sample is firstly analyzed by the standard CF-LIBS approach to obtain the estimated concentrations of its constitutive elements, which would be different from the certified concentrations. Then the two sets of concentrations can be made to coincide by applying a simple multiplicative transformation on the points on the Boltzmann plot, in which the  $P(\lambda)$  values can be calculated from the transformation process. The characteristics and advantages of the OPC-LIBS approach have been demonstrated on bronze alloys [21] and, steel [22] and mixed sodium chloride samples [23].

In this work, we compare the results of calculations using CF-LIBS and OPC-LIBS for major and minor constituents of seven certified Ti–6Al–4V alloys, which are the widely used titanium alloys for AM to date. For both CF-LIBS and OPC-LIBS analyses, a Saha-Boltzmann plot with a combination of Saha ionization and Boltzmann excitation distributions to cover a wide upper level energetic range was used to obtain more accurate  $T_{\text{exc}}$  and  $n_e$  to get a more accurate quantitative analysis result.

## 2 Experimental set-up

The experimental set-up has been reported in our previous works [24]. A Q-switched Nd:YAG laser (Brilliant Eazy, Quantel), delivering up to 120 mJ at 1064 nm with a 5 ns pulse duration, was used as the ablation source. The laser operated at a repetition rate of 2 Hz for the overall experiments. The laser beam was directed normal to the sample surface by a dichroic mirror (DMSP950, Thorlabs) and focused over the sample surface using a plano-convex lens ( $f=75$  mm). The focus position of the incident laser was optimized at 6 mm below the sample surface, which was chosen to avoid background gases breakdown. The spot diameter was estimated to be approximately 600  $\mu\text{m}$  by measuring that of the ablation crater. The pulse energy after the focusing lens was 105 mJ measured by a laser power meter (842-PE, Newport). The laser power density on the sample surface was approximately  $7.43 \text{ GW/cm}^2$ , which lead to the establishment of stoichiometric ablation [25–27].

The optical emission of the laser-induced plasma was collected with a quartz lens ( $f=100$  mm), and transported via an optical fiber of 200  $\mu\text{m}$  core diameter. The fiber was coupled to an Echelle spectrograph (with spectral resolving power  $\lambda/\Delta\lambda=12,500$ ) coupled with an intensified CCD camera (iStar DH334T, Andor). The collection optical axis

was fixed at a  $45^\circ$  angle to the laser propagation axis. The timing of the whole system was managed by a computer that controls the laser pulse, the star and the width of the ICCD acquisition gate after a suitable delay, and the spectral data transfer towards the computer. In the acquisition of the spectra, the gating of the spectrometer was set at delay time  $t_d=5 \mu\text{s}$  and gate width  $t_g=2 \mu\text{s}$  for a relatively high signal in a regime where space and time variation of plasma parameters are almost negligible.

The reference titanium alloy samples here used are provided by China Shipbuilding Industry Group Co., Ltd. and their certified compositions are listed in Table 1. The concentration of aluminum ranged from 5.66 to 11.48 at.%, while the concentration of vanadium ranged from 2.65 to 5.21 at.%. This kind of  $\alpha$ - $\beta$  alloy Ti–6Al–4V has received prime attention as the benchmark titanium alloy because of its broad applications in industry and the associated high cost of manufacturing and long lead time [28, 29].

## 3 Results and discussion

A typical LIBS spectrum corresponding to the Sample 2 is shown in Fig. 1, which was averaged over ten laser shots. Both standard CF-LIBS and OPC-LIBS approaches rest on the underlying hypotheses of stoichiometric ablation, local thermal equilibrium (LTE), spatially homogeneous and optically thin plasma, which are necessary to design self-consistent algorithms. In the OPC-LIBS analyses, Sample 2 was selected as the standard of known composition, while other six samples were considered as unknown. The lines used for the comparison investigation between CF-LIBS and OPC-LIBS methods are reported in Table 2 and their transition probabilities were obtained from the National Institute of Standards and Technology (NIST) database. The comprehensive correction factors  $P(\lambda)$  calculated with the Sample 2 are shown in Table 2.

For both CF-LIBS and OPC-LIBS analyses, plasma temperature ( $T_{\text{exc}}$ ) and electron density ( $n_e$ ) are important and essential physical parameters. A Saha–Boltzmann plot with a combination of Saha ionization and Boltzmann excitation distributions to cover a wide upper level energetic range

**Table 1** The standard reference titanium alloy samples used for the analysis (elemental concentration in at. %)

Sample	Ti	Al	V
1	91.70	5.66	2.65
2	88.73	6.23	5.03
3	87.99	6.79	5.21
4	87.35	8.07	4.58
5	87.68	9.22	3.10
6	85.74	10.59	3.67
7	85.07	11.48	3.45

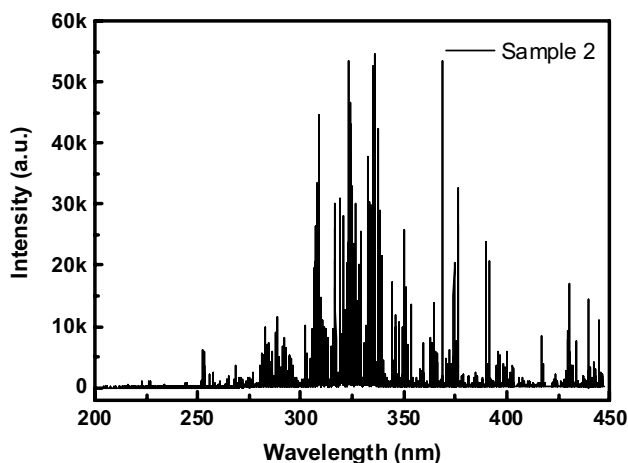


Fig. 1 LIBS spectrum of sample 2

Table 2 Lines used for the CF-LIBS and OPC-LIBS analyses. The lines marked with an asterisk were also used for classical LIBS analysis based on calibration curves

Species	Wavelength (nm)/(P(λ))		
Ti I	364.267 (1.107)	365.350 (0.604)*	375.286 (1.104)
	398.970 (1.002)	399.860 (0.965)	
Al I	308.215 (3.490)	394.401 (1.028)*	396.152 (1.017)
V I	318.399 (4.517)	411.178 (1.078)	437.923 (0.840)*
	438.471 (2.027)	438.998 (0.856)	
Ti II	307.522 (0.638)	307.865 (0.490)	315.419 (1.387)
	315.567 (1.657)	320.253 (0.957)	322.424 (1.075)
	324.198 (0.601)	332.676 (1.269)	333.211 (0.856)
	340.242 (1.043)	345.638 (0.870)	347.718 (1.018)
V II	270.094 (1.881)	290.881 (1.740)	296.837 (1.393)
	310.229 (1.421)	312.528 (1.298)	313.652 (1.248)

was used to obtain more accurate  $T_{exc}$  and  $n_e$ . Plotting the logarithmic ratio of several atomic and ionic emission line combinations as a function of their energy differences results in a line whose slope is inversely proportional to  $T_{exc}$  [30]:

$$\ln \left( \frac{I_{mn}^{II} F(\lambda) A_{ij}^I g_i^I}{I_{ij}^I F(\lambda) A_{mn}^{II} g_m^{sII}} \right) = - \frac{(E_m^{II} - E_i^I + E_{ion})}{kT_{exc}} + \ln \left( \frac{2(2\pi m_e kT_{exc})^{3/2}}{n_e h^3} \right), \tag{1}$$

where the indices I and II differentiate the atomic and first ionized species, respectively;  $m_e$ ,  $h$  and  $E_{ion}$  are the mass of an electron, the Planck’s constant, and the 1st ionization energy of the element of interest, respectively. Using this linear regression to calculate  $T_{exc}$  is less sensitive to LIBS measurement noise. Figure 2 shows the Saha–Boltzmann plots of Ti I-II spectral lines of Sample 2 before and after

OPC corrections. It was found that the plasma temperatures were the same value of 11,022 K. The OPC corrections did not change the  $T_{exc}$  calculation, and re-adjusted the scattered points in the Saha–Boltzmann plot to a perfectly linear distribution. Furthermore, the electron density can also be obtained from the intercept of the Saha–Boltzmann plots. The electron densities obtained before and after application of OPC corrections were the same value of  $1.014 \times 10^{17} \text{ cm}^{-3}$ . The McWhirter criterion is a necessary, though insufficient, condition for LTE, and is widely used in LIBS analysis. The condition that atomic and ionic states should be populated and depopulated dominantly by electron collisions, rather than by radiation processes, requires an electron density which is sufficient to ensure a high collision rate [31]. In our experimental conditions, the laser-induced plasma was considered spatially stationary and homogeneous. The corresponding lower limit of electron density  $N_e$  ( $\text{cm}^{-3}$ ) is expressed through this criterion:

$$N_e \geq 1.6 \times 10^{12} T^{1/2} (\Delta E)^3, \tag{2}$$

where  $T$  (K) is the plasma temperature and  $\Delta E$  (eV) is the largest energy gap between adjacent levels of the considered elements. In this case, for a plasma largely dominated by Ti, V and Al atoms and ions  $\Delta E$  is maximized for V II ( $\Delta E=4.589 \text{ eV}$ ). Under the plasma temperature of 11,022 K, the lower limit of electron density  $N_e$  is  $1.623 \times 10^{16} \text{ cm}^{-3}$ . The electron density calculated from the intercept of the coupled Saha–Boltzmann plot is much higher than this limit implying that the LTE approximation for the CF-LIBS analysis is valid. The relationship between plasma parameters ( $T_{exc}$  and  $n_e$ ) and concentration of titanium in the samples are shown in Fig. 3. The plasma temperature is approximately constant at about 11,000 K for the investigated seven samples. While the electron density shows a slight decrease from  $1.02 \times 10^{17} \text{ cm}^{-3}$  for 85.07 at. % Ti sample to  $7.83 \times 10^{16} \text{ cm}^{-3}$  for 91.70 at. % Ti sample. These electron densities calculated using Saha–Boltzmann plots is nearly 5.5 times larger than the critical electron densities calculated by the McWhirter criterion.

Figure 4 shows the Boltzmann plots constructed with and

without OPC corrections for Samples 2, 4 and 7, respectively. The left column (a, c, e) shows the Boltzmann plots used for conventional CF-LIBS while the right column (b, d, f) shows the OPC-LIBS results. In Fig. 4, the solid lines are the least squares linear fitting to the data points. Without the OPC correction, the obtained original lines, compromised by self-absorption and uncertainties associated with  $A_{ij}$  and

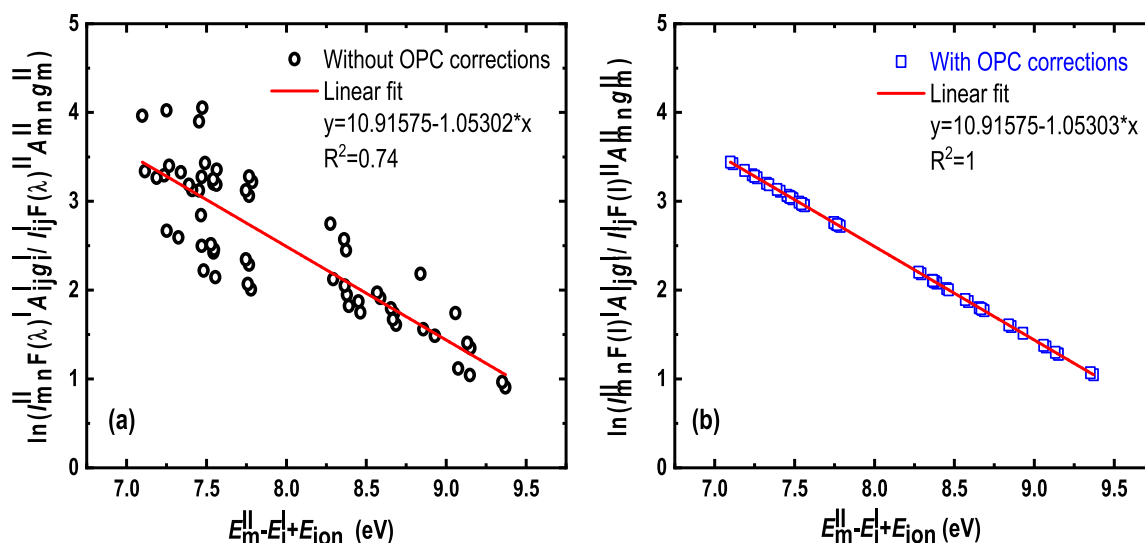


Fig. 2 Saha-Boltzmann plots of Ti III/I **a** without and **b** with OPC correction for the sample 2. Straight lines represent the linear fit of the points

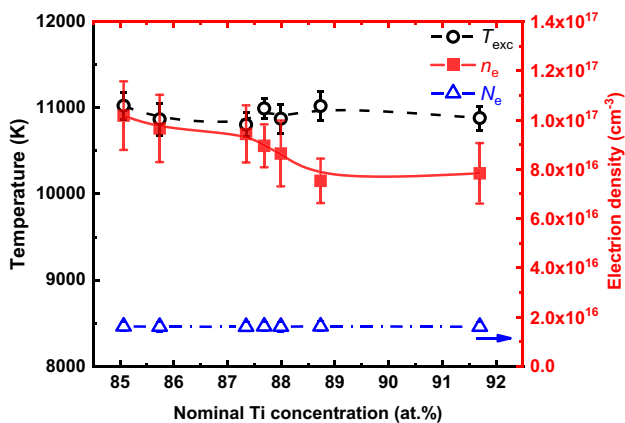


Fig. 3 Plasma temperature (circles) and electron density (squares) as a function of Ti concentration calculated using Saha-Boltzmann plots with OPC corrections. The critical electron density (triangle) as a function of Ti concentration estimated by the McWhirter criterion

$F(\lambda)$ , make the points on Boltzmann plots in a relatively scattered pattern, and the coefficient of determination of the linear fitting curve is lower. Furthermore, the slope of Al I and V I were contrary to expectations due to the strong self-absorption. Consequently, the linear fitting (dashed lines) with the fixed slope of Ti II data were used for the data of Al I and V I in traditional CF-LIBS analyses. After performing the correction using the proposed OPC-LIBS method, as shown in Fig. 4b, d and f, the linearity of the points corresponding to atoms and ions of Ti and V were significantly improved. It can be seen that the effect of OPC corrections for standard and “unknown” samples were very similar.

The comparison results of CF-LIBS and OPC-LIBS procedure are reported in Table 3 and in Fig. 5. One spectrum

of Sample S2 was used as the standard for OPC-LIBS procedure to rescale the line emission intensity in atomic percent. In Table 3, the fourth and fifth columns show the mean values from ten quantitative calculations for each sample by CF-LIBS and OPC-LIBS, respectively. It was found that the quantitative results are more deviated from the reference values for traditional CF-LIBS method without corrections. For OPC-LIBS method, the concentrations calculated on the major and the minor elements remarkably close to the reference values with a better stability. The accuracy is often expressed as percent relative error. The much smaller relative error of predicted concentration indicates that the OPC-LIBS method permits a much reliable quantitative analysis capability. Figure 5 shows the comparison of the predicted concentrations by OPC-LIBS (stars), by CF-LIBS (circles) and by conventional LIBS methods (squares) vs. the certified concentrations. The concentrations calculated by OPC-LIBS on the ‘unknown’ samples are very close to the certified concentrations. The error bars correspond to the standard deviation of ten replicate measurements. Figure 5 presents the relevant calibration curves using absolute intensity for V I (437.92 nm), Al I (394.40 nm) and Ti I (365.35 nm) in titanium alloys. It is found that only the signal intensity of V varies linearly at the low concentrations. One clearly sees that the calibration curves do not vary linearly with the Al concentration of 5.66 at.%—11.48 at.% in the matrix, the nonlinearity problem being much worse for the major element of Ti. This deviation at higher concentration of the calibration curves of Al and Ti from the linear relationship results from self-absorption due to the resonant character of the lines considered here [24] In OPC-LIBS methods, the total number density of the element of interest is obtained by summing over the neutral and

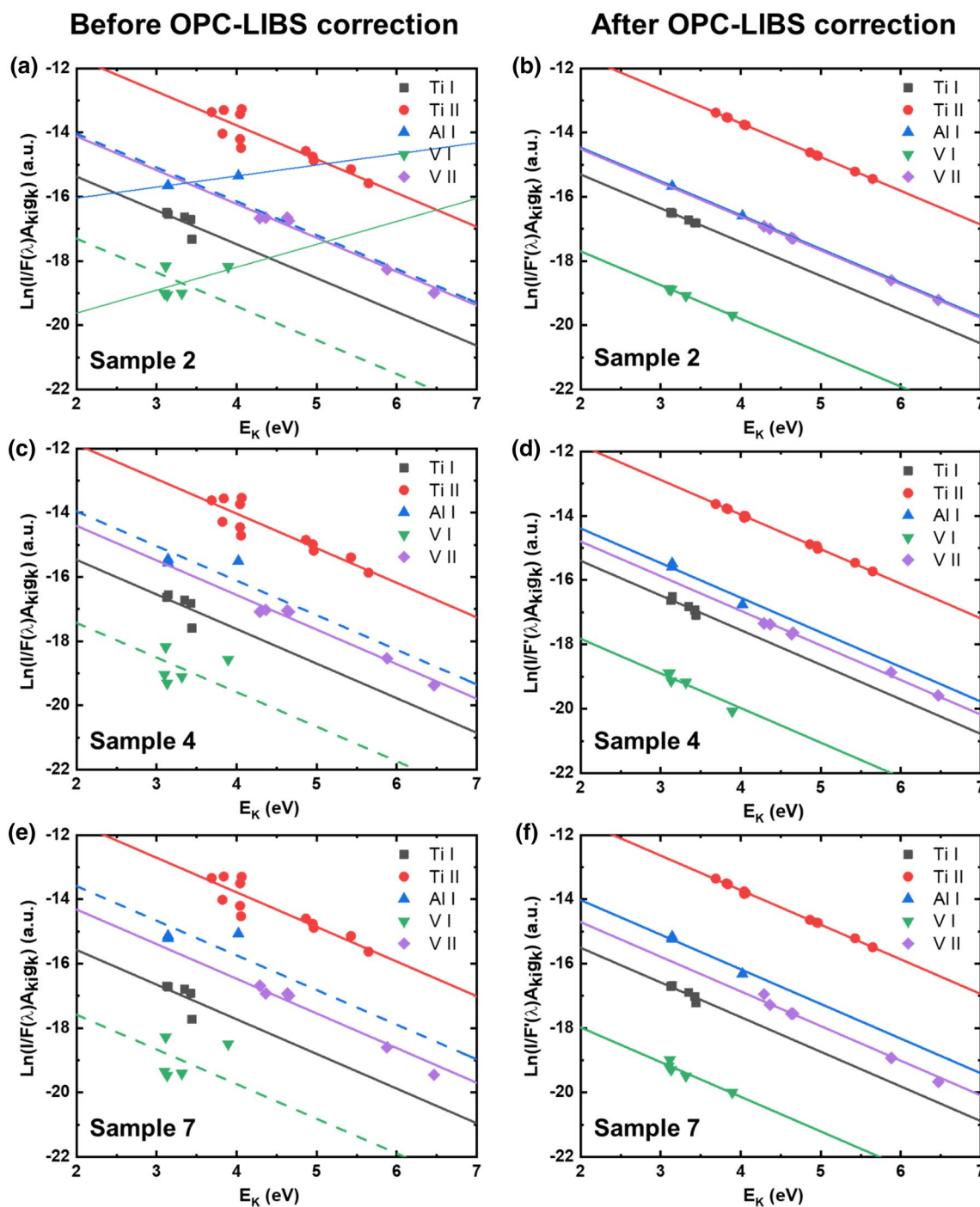


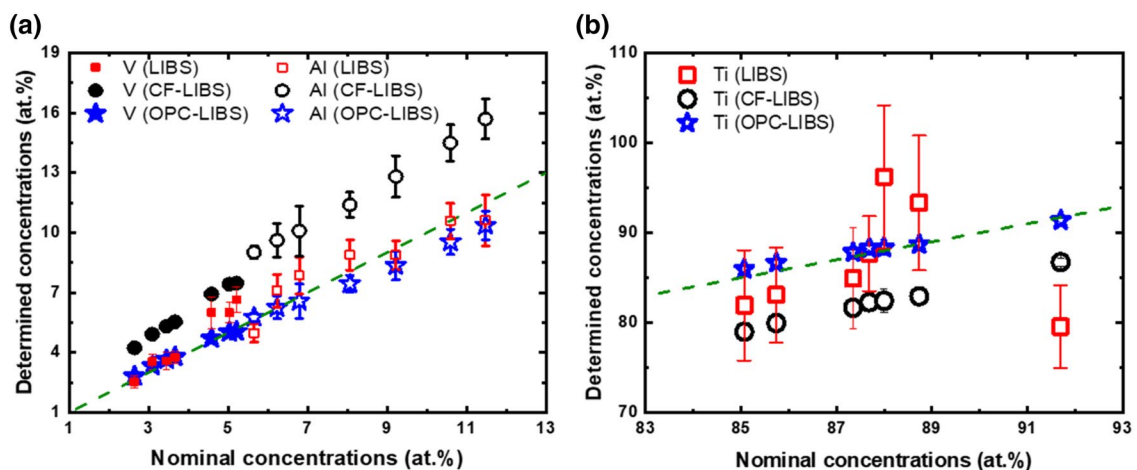
Fig. 4 Boltzmann plots obtained before and after OPC-LIBS for Sample 2 (top), Sample 4 (middle) and Sample 7 (bottom)

the ionization states. Typically, this includes neutral (I) and singly ionized (II) species. Once the total number densities have been calculated for all the elements, the relative abundance of each element is obtained in terms of molar fractions. The results of OPC-LIBS analyses show perfect linear responses of experimentally determined concentrations to the nominal concentrations for all elements. By linear fitting

of OPC-LIBS results, the  $R^2$  of the correlations were 0.993 for V, 0.938 for Al and 0.986 for Ti, respectively. It is evident that the OPC-LIBS procedure leads to a more accurate determination of the titanium alloy composition compared with the CF-LIBS approach and the classical calibration curve technique. It was found that the OPC-LIBS is not much effective in improving the precision. Since the OPC-LIBS

**Table 3** Quantitative results of nominal compositions of samples with the CF-LIBS and OPC-LIBS

Sample	Element	Concentration (at.%)			Relative error (%)	
		Reference	CF-LIBS	OPC-LIBS	CF-LIBS	OPC-LIBS
S1	Ti	91.70	86.7±0.5	91.4±0.3	5.45	0.33
	Al	5.66	9.0±0.3	5.8±0.2	59.0	2.47
	V	2.65	4.2±0.3	2.8±0.2	58.5	5.66
S2	Ti	88.73	82.9±1.0	88.7±0.7	6.57	0.03
	Al	6.23	9.6±0.8	6.3±0.6	54.1	1.12
	V	5.03	7.4±0.3	5.1±0.2	47.1	1.13
S3	Ti	87.99	82.4±1.3	88.4±0.9	6.35	0.47
	Al	6.79	10.1±1.3	6.6±0.9	48.7	2.80
	V	5.21	7.5±0.3	5.1±0.2	44.0	2.11
S4	Ti	87.35	81.7±0.7	87.8±0.5	6.47	0.52
	Al	8.07	11.4±0.6	7.5±0.4	41.3	7.06
	V	4.58	6.9±0.3	4.7±0.2	50.7	2.62
S5	Ti	87.68	82.3±1.1	88.3±0.8	6.14	0.71
	Al	9.22	12.8±1.0	8.4±0.7	38.8	8.89
	V	3.10	4.9±0.2	3.3±0.1	58.1	6.45
S6	Ti	85.07	79.0±0.9	86.0±0.7	7.14	1.09
	Al	11.48	15.7±1.0	10.4±0.7	36.8	9.41
	V	3.45	5.3±0.2	3.7±0.2	53.6	7.25
S7	Ti	85.74	80.0±0.9	86.7±0.7	6.69	1.12
	Al	10.59	14.5±0.9	9.5±0.6	36.9	10.3
	V	3.67	5.5±0.2	3.8±0.1	49.9	3.54

**Fig. 5** Comparison of the predicted concentrations determined by OPC-LIBS (stars), by CF-LIBS (circles) and by conventional calibration curve method (squares) vs. the certified concentrations. The

green dashed line corresponds to the ideal correspondence between nominal concentration and that predicted by LIBS

method empirically determines a correction factor, namely  $P(\lambda)$ , applied to correct the intensity of each emission of species used in the Boltzmann plot.  $P(\lambda)$ , a series of fixed values, cannot effectively suppress the random fluctuation of plasma emission. In addition, the relative error increases slightly for high Al concentration in the OPC-LIBS method. The main cause is the self-absorption of Al lines. In the spectral range of 240–440 nm only three clearly identifiable

Al resonance atomic lines can be used to construct Boltzmann plots. The severe self-absorption effect weakens the peak of Al line, and reduces the predicted concentration of Al. The number density of singly ionized aluminum was calculated from the number density of Al atoms by Saha's equation, and underestimated due to the self-absorption effect of Al atomic lines. The compensation of self-absorption given by the OPC-LIBS method is partial, and other methods for

compensating the self-absorption will be investigated in the further.

## 4 Conclusion

The potential usefulness of OPC-LIBS method combined with a Saha-Boltzmann plot to calculate the plasma temperature and electron density have been demonstrated. The OPC-LIBS maintains the advantage of the CF-LIBS method in terms of independence on the matrix effect while offering a more accurate analytical performance. In this work, the application of the OPC-LIBS procedure to a set of certified titanium alloy samples has resulted in a significant improvement of the composition results for both major and minor constituents, with respect to those obtained in the conventional calibration curve and CF-LIBS approach. This new method provides a simple and low-cost way for rapid *in-situ* quantitative multi-elemental analysis in the additive manufacturing process.

**Acknowledgements** This research was supported by the National Key R&D Program of China (No. 2017YFE0301304), the National MCF Energy R&D Program of China (No. 2019YFE03080100), the National Natural Science Foundation of China (Nos. 11705020, 51837008, 11861131010), China Postdoctoral Science Foundation (Nos. 2018M630285, 2019M661087), Fundamental Research Funds for the Central Universities (Nos. DUT19RC(4)031, DUT18TD02) and Project SKLD18KM12 supported by China State Key Lab. of Power System.

## References

1. R.R. Boyer, Mater. Sci. Eng. A-Struct. Mater. Prop. Microstruct. Process. **213**, 103 (1996)
2. D. Herzog, V. Seyda, E. Wycisk, C. Emmelmann, Acta Mater. **117**, 371 (2016)
3. L. Song, W. Huang, X. Han, J. Mazumder, IEEE Trans. Ind. Electron. **64**, 633 (2017)
4. V.N. Lednev, P.A. Sdvizhenskii, R.D. Asyutin, R.S. Tretyakov, M.Y. Grishin, A.Y. Stavertiy, A.N. Fedorov, S.M. Pershin, Opt. Express **27**, 4612 (2019)
5. Z. Wang, T.-B. Yuan, Z.-Y. Hou, W.-D. Zhou, J.-D. Lu, H.-B. Ding, X.-Y. Zeng, Front. Phys. **9**, 419 (2014)
6. D.W. Hahn, N. Omenetto, Appl. Spectrosc. **66**, 347 (2012)
7. A. Ciucci, M. Corsi, V. Palleschi, S. Rastelli, A. Salvetti, E. Tognoni, Appl. Spectrosc. **53**, 960 (1999)
8. S.M. Pershin, F. Colao, V. Spizzichino, Laser Phys. **16**, 455 (2006)
9. M.L. Shah, A.K. Pulhani, G.P. Gupta, B.M. Suri, Appl. Opt. **51**, 4612 (2012)
10. H. Fu, F. Dong, H. Wang, J. Jia, Z. Ni, Appl. Spectrosc. **71**, 1982 (2017)
11. A. Jabbar, Z. Hou, J. Liu, R. Ahmed, S. Mahmood, Z. Wang, Spectrochim. Acta Part B At. Spectrosc. **157**, 84 (2019)
12. M. Corsi, G. Cristoforetti, M. Hidalgo, S. Legnaioli, V. Palleschi, A. Salvetti, E. Tognoni, C. Vallebona, Appl. Opt. **42**, 6133 (2003)
13. S. Pandhija, A.K. Rai, Appl. Phys. B Lasers Opt. **94**, 545 (2009)
14. A. Jabbar, M. Akhtar, A. Ali, S. Mehmood, S. Iftikhar, M.A. Baig, Optoelectron. Lett. **15**, 57 (2019)
15. M. Corsi, G. Cristoforetti, M. Hidalgo, S. Legnaioli, V. Palleschi, A. Salvetti, E. Tognoni, C. Vallebona, Appl. Geochem. **21**, 748 (2006)
16. R. Kumar, A.K. Rai, D. Alamelu, S.K. Aggarwal, Environ. Monit. Assess. **185**, 171 (2013)
17. K. Ibano, D. Nishijima, Y. Ueda, R.P. Doerner, J. Nucl. Mater. **522**, 324 (2019)
18. F. Colao, R. Fantoni, V. Lazic, A. Paolini, F. Fabbri, G.G. Ori, L. Marinangeli, A. Baliva, Planet. Space Sci. **52**, 117 (2004)
19. G.S. Senesi, G. Tempesta, P. Manzari, G. Agrosi, Geostand. Geoenal. Res. **40**, 533 (2016)
20. A. Kramida, Y. Ralchenko, J. Reader, NIST ASD Team, (National Institute of Standards and Technology, Gaithersburg, 2019).
21. G. Cavalcanti, D. Teixeira, S. Legnaioli, G. Lorenzetti, L. Pardini, V. Palleschi, Spectrochim. Acta Part B **87**, 51 (2013)
22. H. Fu, H. Wang, J. Jia, Z. Ni, F. Dong, Appl. Spectrosc. **72**, 1183 (2018)
23. L.C.L. Borduchi, D.M.B.P. Milori, P.R. Villas-Boas, Spectrochim. Acta Part B **160**, 105692 (2019)
24. R. Hai, Z. He, X. Yu, L. Sun, D. Wu, H. Ding, Opt. Express **27**, 2509 (2019)
25. T.C. Wing, R.E. Russo, Spectrochim. Acta Part B At. Spectrosc. **46**, 1471 (1991)
26. X. Mao, W.-T. Chan, M. Caetano, M.A. Shannon, R.E. Russo, Appl. Surf. Sci. **96**, 126 (1996)
27. R.E. Russo, Appl. Spectrosc. **49**, A14 (1995)
28. L. Thijs, F. Verhaeghe, T. Craeghs, J. Van Humbeek, J.P. Kruth, Acta Mater. **58**, 3303 (2010)
29. W. Xu, M. Brandt, S. Sun, J. Elambasseril, Q. Liu, K. Latham, K. Xia, M. Qian, Acta Mater. **85**, 74 (2015)
30. A.W. Miziolek, V. Palleschi, I. Schechter, *Laser Induced Breakdown Spectroscopy* (Cambridge University Press, Cambridge, 2006).
31. R.H. Huddleston, S.L. Leonard, *Plasma Diagnostic Techniques* (Academic Press, New York, 1965).

**Publisher's Note** Springer Nature remains neutral with regard to jurisdictional claims in published maps and institutional affiliations.